Binding of Cholera Toxin B-Subunit to a Ganglioside GM1-Functionalized PEG-Tethered Lipid Membrane

Erik B. Watkins,* Andrew J. C. Dennison, and Jaroslaw Majewski

Cite This: *Langmuir* 2022, 38, 6959–6966

Read Online

ACCESS | Metrics & More | Article Recommendations

ABSTRACT: We report neutron reflectometry (NR) studies of polyethylene glycol (PEG)-tethered model lipid membranes at the solid−liquid interface and of cholera toxin's B-subunit (CTxB) binding to tethered membranes containing ganglioside GM1 receptors. First, tethered polymer brushes were formed by grafting silane-functionalized PEG lipopolymers to quartz from solution. Subsequent deposition of lipids by Langmuir−Blodgett/Langmuir−Schaefer (LB/LS) resulted in a tethered bilayer structure separated from the solid support by a hydrated PEG layer. NR revealed that the tethers formed a highly hydrated polymer brush, uniformly separating the bilayer from the underlying solid substrate. Further, the lipid bilayer did not significantly perturb the brush's conformation relative to a free brush. Biological functionality of the tethered bilayers was verified by interacting CTxB, with ganglioside GM1 receptors incorporated into the bilayer. The surface coverage of CTxB bound to the lipid membrane, $\theta_{CTB}= 0.58 \pm 0.08$, was consistent with the coverage predicted for random sequential absorption, and toxin binding did not impact the membrane conformation.
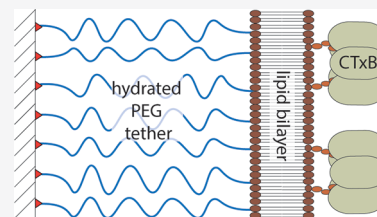
INTRODUCTION

Many biophysical studies of transmembrane proteins and lipid−protein interactions are limited by difficulties in the reliable creation of model bio-mimetic membranes in their natural liquid environment. Frequently, lipid monolayers at the liquid−air interface,[1−3] lipid nanodiscs,[4,5] and solid-supported lipid bilayers[6−8] provide good model systems to study protein−lipid interactions. The ability to apply surface sensitive biophysical methods to the study of planar model membranes (e.g. lipid monolayers and solid supported bilayers) enables access to otherwise unobtainable detailed structural information. However, lipid bilayers in contact with solid substrates suffer from decreased in-plane lipid mobility, suppressed out-of-plane fluctuations, and reduced protein mobility and, in some cases, can promote membrane protein denaturation due to conformational changes at the substrate. The extent to which overall membrane structure and dynamics is altered by interactions with the support also remains unclear. Therefore, the reliable creation of functional and well-characterized lipid bilayer membranes at solid−liquid interfaces attracts significant experimental effort.[9] A highly hydrated layer separating the membrane from the solid substrate is one strategy to alleviate these effects and allow structural characterization of the membrane systems under more biologically relevant conditions. In many cases, it is also a prerequisite for studying membrane proteins. To fabricate such functional lipid membrane architectures, a large research effort has been directed toward engineering polymeric layers separating the lipid bilayer from an underlying solid support.[10−20] Previous work has followed a wide variety of design philosophies using diverse cushioning or tethering

materials to either mimic specific environments,[21] facilitate specific experimental techniques,[22] or control particular aspects of the membrane.[23] PEG derivatives remain one of the principal choices to create tethered bilayer membranes due to their wide availability with diverse terminal functionalization, high solubility in water, lack of charge, and anti-fouling properties.

Here, neutron reflectometry was used to investigate the structure of membranes tethered to quartz substrates via silane-functionalized polyethylene glycol (PEG) lipopolymers. The PEG lipopolymer-tethering molecules (DSPE−PEG$_{75}$−silane) consisted of a triethoxysilane termination to enable covalent bonding to silica surfaces, a 75 monomer length PEG polymer chain, and a DSPE lipid termination to enable integration into a lipid bilayer environment. Tethered bilayers were formed by first reacting the silane-functionalized lipopolymer with a quartz surface from 1:1 MeOH:EtOH solution and by subsequently completing the lipid bilayers via Langmuir−Blodgett/Langmuir−Schaefer deposition (Figure 1).[24] Neutron reflectometry revealed that this simple procedure was capable of forming tethered lipid bilayers with near-complete surface coverage and uniform separation from the solid support when high tether densities were used. Using the binding of
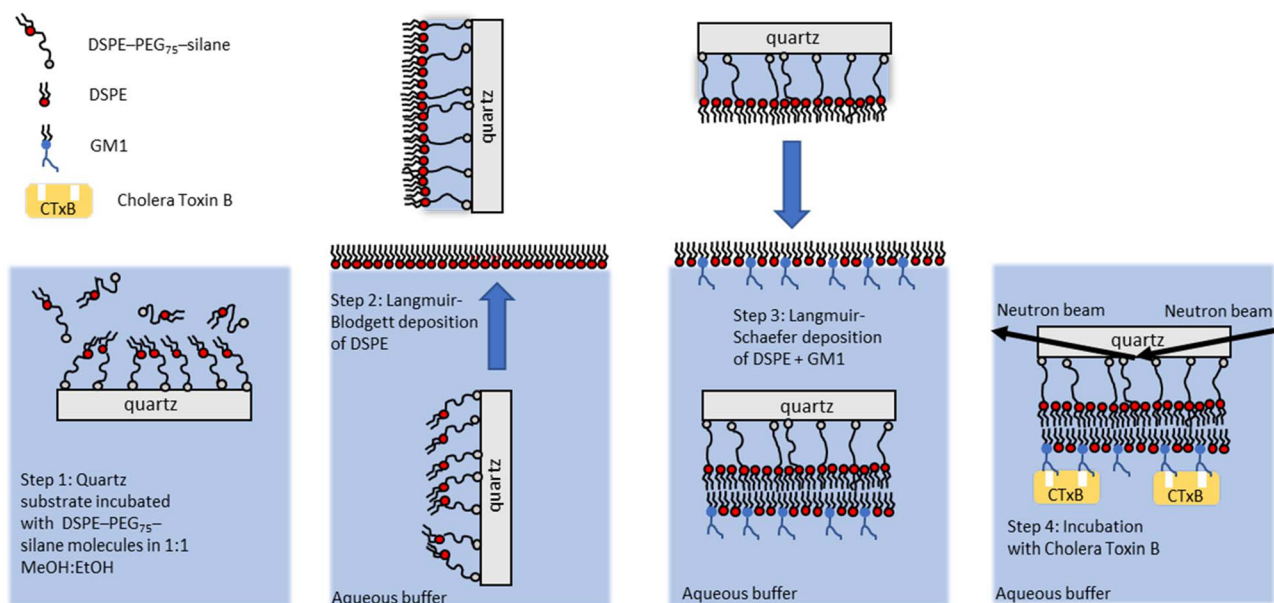
Figure 1. Schematic of the tethered bilayer deposition process and neutron reflectometry measurement geometry. While the cartoon depicts hydration of the tether region between Langmuir−Blodgett (LB) and Langmuir−Schaefer (LS) depositions, it is possible that drying and rehydration of the tethers occurs between these steps.

cholera toxin's B-subunit (CTxB) to membrane-embedded glycolipid receptors, we demonstrate the suitability of this system for studying lipid−toxin interactions.

EXPERIMENTAL SECTION

Materials. DSPC, tail-deuterated DSPC (d-DSPC), and ganglioside GM1 (brain, ovine sodium salt; predominantly 18:0 and 20:0 acyl chains on the 18:1 sphingosine base) were purchased from Avanti Polar Lipids, Alabaster, AL, USA and used without prior purification. The deuterated compounds were used to enhance the scattering contrast in neutron experiments. Bifunctionalized 3300 MW PEG chains (75 monomers) with DSPE and triethoxysilane terminations (DSPE−PEG$_{75}$−silane) was purchased from Nanocs, New York, USA. The total MW of the DSPE−PEG$_{75}$−silane molecule is equal to 4369 (3300 MW PEG, 748 MW DSPE, 163 MW ethoxy silane, and the remaining linking the three components). Schematics of the lipid molecules are shown in Figure 2. The CTxB cholera toxin subunit was purchased from Sigma-Aldrich, France and used without additional purification. Aqueous buffers were prepared using solutions of pH 7.4, 150 mM calcium-free phosphate buffer in water (Millipore), or D$_2$O
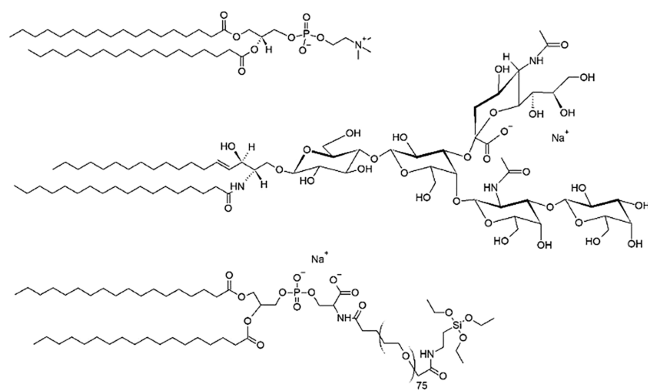

Figure 2. Chemical structures of the molecules used in this work. From top: 1,2-distearoyl-*sn*-glycero-3-phosphocholine (DSPC), GM1, and DSPE−PEG$_{75}$−silane.

(Eurisotop, France). Single-crystal quartz substrates with 3 Å rms roughness were obtained from Crystran, Poole, UK.

Preparation of PEG-Tethered Membranes. Quartz substrates were cleaned by successive sonication in detergent and MilliQ water followed by consecutive rinsing with 2% Gigapur, Millipore purified H$_2$O, and pure ethanol. The ethanol was blown off with ultrapure N$_2$, and the substrates were exposed to UV ozone for 20−40 min. To functionalize the surface with tethered lipids, 1 mM solutions of DSPE−PEG$_{75}$−silane molecules in 1:1 MeOH:EtOH mixture were prepared and used within 10 min. While this solvent was chosen to simplify sample preparation, it yielded incomplete solvation of the DSPE−PEG$_{75}$ − silane molecules. Freshly cleaned quartz substrates were incubated with the solution for >12 h.

Lipid bilayers with leaflets composed of DSPC, d-DSPC, or 90:10 d-DSPC:GM1 were formed by depositing the lipids on DSPE−PEG$_{75}$-functionalized surfaces using the Langmuir−Blodgett/Langmuir−Schaefer (LB/LS) technique.[24] DSPC (1,2-distearoyl-*sn*-glycero-3-phosphocholine) lipids were used to complete the bilayer to match the hydrocarbon chain length of the lipopolymer DSPE termination. For studies involving CTxB protein interaction, ganglioside GM1 receptors were included in the lipid bilayer to enable protein binding. Lipid mixtures used for LB/LS deposition were dissolved in chloroform at 1 mg/mL and spread onto a Millipore purified water subphase in a Langmuir trough (Nima, UK) using a microsyringe. Solvent was allowed to evaporate for at least 10 min prior to area compression to a surface pressure of 40 mN/m. After equilibrating for at least 10 min, the inner leaflet was LB-deposited by lifting the substrate at a rate of 1−2 mm/min, and the outer leaflet was LS-deposited by lowering the substrate through the monolayer at a faster rate of 10 mm/min (Figure 1). For studies involving CTxB binding, CTxB was injected into the solid−liquid cell at a concentration of 10 mg/L and incubated with the membrane for 5 h before exchanging the liquid for NR measurement.

Neutron Reflectivity. Neutron reflectivity (NR) measurements were performed using the FIGARO beamline[25] at the Institute Laue-Langevin in Grenoble, France. Reflectivity, *R*, is defined as the ratio of the number of neutrons elastically and specularly scattered from a surface to that of the incident beam and is measured as a function of momentum transfer normal to the surface ($Q_z = |k_{out}-k_{in}| = 4\pi\sin\theta/\lambda$), where θ is the angle of incidence and λ is the neutron wavelength. Here, we have chosen to display the reflectivity data multiplied by Q_z^4 to compensate for the sharp decrease in the reflectivity as described
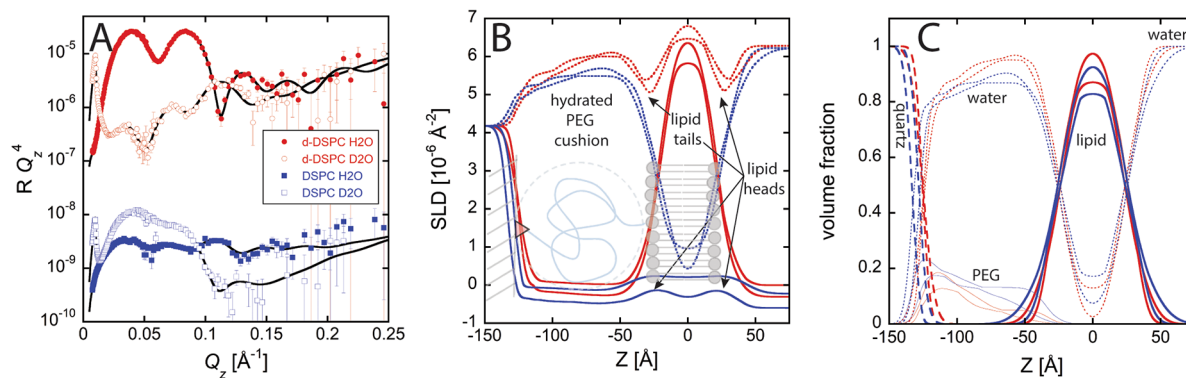
Figure 3. (A) NR (symbols with error bars) obtained for lipopolymer-tethered membranes composed of DSPC (blue squares) and d-DSPC (red circles) bilayers supported on highly hydrated PEG cushions and measured in both H_2O (solid symbols) and D_2O (open symbols) subphases. Solids lines are best fits to the data corresponding to the SLD and volume fractions presented. Data and fits for d-DSPC have been offset vertically for clarity. (B) Red lines correspond to SLD distributions of d-DSPC and blue lines to h-DSPC with solid lines corresponding to measurements in H_2O and dashed lines to measurements in D_2O. Pairs of matched lines define regions of SLD that satisfy the χ^2_{min} + 1 criteria and represent the uncertainty of the distribution. A schematic is overlaid with the SLD profile to show the positions of different structural elements of the system. (C) Volume fractions of individual components, assuming each model layer corresponds to a mixture of a single tether component and water, were obtained through the co-refinement of H_2O and D_2O contrasts. Solid lines correspond to the lipid membrane, dotted lines correspond to water, thin lines correspond to PEG, and dashed lines correspond to the substrate. In (B) and (C), the center of the lipid bilayer was defined as Z = 0.

by Fresnel's law: $R \approx Q_z^{-4}$. Using neutron wavelengths from 2 to 20 Å, values of the momentum transfer, Q_z, up to 0.20 Å^{-1} at a resolution dQ_z/Q_z of 7% and reflectivities down to $R \approx 5 \times 10^{-7}$ were measured. The coherent area of the neutron beam projected onto the sample is approximately 1 × 100 μm, and the data is an average of the reflectivity from all coherent regions within the beam footprint (approximately 30 × 75 mm^2). In all cases presented in this study, the neutron beam penetrated through the quartz support to be scattered from the model membranes at the solid−liquid interface.

The reflectivity curve contains information regarding the sample-normal profile of the in-plane averaged nuclear scattering length density (SLD). From the measured reflectivity profile, the thickness, SLD, and roughness of a series of layers normal to the substrate can be determined by minimizing the difference between the measured reflectivity and that obtained from a modeled SLD profile. Generally, reflectivity experiments only measure intensities and phase information is not obtained. Therefore, the transformation of the data from reciprocal space to real space is not unique. Limiting the possible solutions through constraints based on known chemical identities of layers, expected thickness, and analysis of multiple data sets is extremely helpful for ensuring a physically significant determination of the sample structure. In this work, analysis of NR data was performed by fitting the reflectivity profile of a real-space model to the measured reflectivity curve using box models.[26] Convolution with the 7% dQ_z/Q_z instrumental resolution did not significantly impact the calculated reflectivity profiles and was not performed when fitting the data. Implementing the Parratt formalism, box models described the SLD distribution as a sequence of *n* constant SLD slabs. Error functions were used to connect adjoining slabs and describe interfacial roughness. The SLD profiles shown in the text are the final curves after the interfacial roughness was applied to the box profiles. In all cases, multiple contrasts were co-refined using the same model to yield the highest confidence in the interfacial structure.

All systems studied here were measured using multiple neutron scattering contrast conditions. The polymer-supported lipid membranes were measured against (i) deuterated water, D_2O, and (ii) H_2O as liquid subphases. In these cases, the liquid subphase was exchanged in situ from H_2O to D_2O, and the NR was measured. Cushioned bilayers created from both hydrogenated (h-DSPC) and deuterated (d-DSPC) phospholipids were also investigated to provide complementary contrast conditions. Due to the added complexity of the system, the interaction of CTxB with polymer-cushioned d-DSPC bilayers were performed using three different contrast conditions: (i),

(ii), and (iii) where the liquid-subphase SLD was matched to quartz (CMW). Reflectivity data were fit using a custom code. All contrasts for the same system were simultaneously refined using a numerical least-square fitting procedure, which significantly increased the confidence in the resulting SLD distributions. Layer thicknesses were constrained to be greater than or equal to twice the roughness sigma values at its interfaces to obtain physically relevant parameterizations of the SLD profile. A Levenburg−Marquardt minimization algorithm was used to vary the box model parameters to obtain the solution corresponding to the lowest χ^2 value. Parameter errors were determined by incrementing the parameter of interest while allowing all others to fit until χ^2 increased by one from the minimum χ^2 value (χ^2_{min} + 1). This procedure yielded several hundred fits satisfying the χ^2_{min} + 1 condition and was used to generate bounds for the uncertainty in the modeled SLD and volume fraction distributions. The theoretical SLD values for densely packed h- and d-DSPC hydrocarbon tails can be estimated as −0.33 × 10^{-6} and 7.2 × 10^{-6} Å^{-2}, respectively. Deuterated water (SLD = 6.34 × 10^{-6} Å^{-2}) maximized the neutron SLD contrast between the hydrogenated lipids and hydrated regions of the sample: high-SLD regions are attributed to water (and highly hydrated PEG), while low-SLD regions correspond to the hydrocarbon lipid tails. For experiments using H_2O (SLD = −0.56 × 10^{-6} Å^{-2}) and deuterated lipids, high-SLD regions can be attributed to the lipids and low-SLD regions correspond to hydrated parts of the system. Generally, the SLD of multicomponent systems is a linear combination of the SLDs of the components scaled by their volume fractions.

■ RESULTS AND DISCUSSION

Tethered Bilayers with Uniform Separation from the Solid Support. Figure 3 shows NR data and corresponding SLD and volume fraction profiles for homogeneously cushioned DSPC (blue) and d-DSPC (red) bilayers, each measured in both D_2O and H_2O subphases. The tethering lipopolymer, DSPE−PEG$_{75}$−silane, was incubated with the quartz substrate for >12 h to provide the highest accessible tether density before depositing the DSPC bilayers leaflets using LB/LS. Panel (A) shows the NR measurements with solid symbols corresponding to H_2O measurements and open symbols to D_2O measurements. Models to describe the tethered membrane consisted of five layers: two to describe the PEG distribution in the cushion, one for the lipid tail

groups, and two symmetric layers corresponding to the lipid head groups. Solid lines in panel (A) correspond to the best-fit SLD distributions presented in panel (B). In panel (B), the SLD distributions of the d-DSPC bilayer are shown in red, and the SLD distributions of the h-DSPC bilayer are shown in blue with solid lines for measurements in H_2O and dashed lines for measurements in D_2O. Estimates of the uncertainty in the SLD distributions are presented by two bounding lines corresponding to the set of models satisfying the $\chi^2_{min} + 1$ metric. The SLD distributions in (B) and the numerical values of the fitting parameters presented in Table 1 clearly indicate the presence

Table 1. Parameters for Fits to Data Presented in Figure 3[a]

	d-DSPC: χ^2 = 5.5−6.5			
Z	SLD	solv	σ	
	4.18*	0*	5.6 ± 1.4	quartz substrate
32.4 ± 3.5[¥]	0.63*	82 ± 4	16.2 ± 3.8	first PEG region
56.5 ± 3.5[¥]	0.63*	97 ± 2	8.2 ± 1.6	second PEG region
16.3 ± 3.1	1.92 ± 1.19	63 ± 13	8.2[•]	inner lipid HGs
39.1 ± 4.8	6.71 ± 0.21	7 ± 6	8.2[•]	alkyl tail region
16.3[‡]	1.92[‡]	63[‡]	8.2[‡•]	outer lipid HGs
	6.28 ± 0.003			D_2O subphase
	−0.16 ± 0.15			H_2O subphases
	h-DSPC: χ^2 = 3.1−4.1			
Z	SLD	solv	σ	
	4.18*	0*	4.8 ± 1.3	quartz substrate
29.7 ± 7.9[¥]	0.63*	78 ± 4	14.8 ± 5.1	first PEG region
60.3 ± 7.9[¥]	0.63*	89 ± 3	10.1 ± 2.6	second PEG region
19.9 ± 5.1	1.33 ± 0.78	65 ± 15	10.1[•]	inner lipid HGs
40.1 ± 10.1	−0.07 ± 0.30	8 ± 8	10.1[•]	alkyl tails region
19.7[‡]	1.33[‡]	65[‡]	10.1[‡•]	outer lipid HGs
	6.22 ± 0.001			D_2O subphase
	−0.41 ± 0.19			H_2O subphase

[a]The units of Z, SLD, and roughness σ are in Å, 10^{-6} Å^{-2}, and Å, respectively. Parameter "solv" describes the volume percent of water in the layer.*Values were fixed to theoretical SLDs. [¥]Values were fixed to theoretical SLDs. [¥]Due to interdependence of the two PEG layer thicknesses, error is given for the total PEG layer. [‡]Fits were constrained to have symmetric lipid headgroups. [•]Roughness of all components of the lipid membrane was constrained to be the same.

of a high-coverage (91 ± 8%) lipid bilayer (low-SLD region for DSPC, high-SLD region for d-DSPC) uniformly separated from the substrate. Volume fractions of the components of the tethered bilayer are shown in panel (C). Comparison of the volume fraction distributions for the DSPC and d-DSPC cases exhibits a high degree of reproducibility in the tethered membrane structure. For the DSPC case, the SLD of the tail region matches the theoretical SLD for gel phase packing within errors. The measured SLD of the d-DSPC tail region is consistent with a mixture of d-DSPC deuterated tails and 3.9−9.2 vol % hydrogenated tails from the DSPE lipopolymer tethers. While the thickness obtained for the lipid head groups is significantly larger than the predicted value of ~10 Å, this is due to the constraint imposed on the model, requiring the layer thickness to be greater than twice the interfacial roughness. As a result, the layers assigned to the head groups correspond to a region that is to some degree a mixture of head groups, water, and lipid tails.

The lipid membrane is separated from the quartz surface by a predominantly uniform 90.5 ± 7.9 Å thick hydrated PEG layer, exhibiting an out-of-plane rms roughness between 6 and 13 Å. Considering the theoretical SLD value of PEG (0.63 × 10^{-6} Å^{-2}) and the measured SLD of the cushion region, the average hydration of the PEG tether region was estimated to be 85−90%. Notably, the fits were significantly improved by dividing the cushion into two regions with different degrees of hydration: reduced hydration (82 ± 6%) near the quartz interface and increased hydration (93 ± 6%) adjacent to the bilayer. This corresponds to a small degree of inhomogeneity of the distribution of the PEG brush with a greater volume fraction of PEG chains adjacent to the solid support.

The tether extension is significantly larger than the PEG$_{75}$ Flory radius ($r_F = aN^{3/5}$ = 47 Å, where N = 75 is the number of PEG monomers and a = 3.5 Å is the monomer length) indicating that the tethers are in the polymer brush regime. The density of MW 3300 PEG is 1.2 g/cm^3, corresponding to a molecular volume of 4566 Å^3. Considering this volume and the degree of hydration and thickness of the tether region, the tether density was estimated to be between 310 and 550 Å^2/chain. For gel-phase DSPC, which has an area per lipid of 46.4 Å^2 at 40 mN/m,[27] this tether density corresponds to approximately 7−12 mol % of the inner leaflet lipids tethered to the quartz surface. This value is in good agreement with the 3.9-9.2 mol % tether composition estimated from the tail region SLD of the d-DSPC-containing tethered membrane. An estimate of the tether density allows comparison of the tether region thickness to the theoretical extension of an equivalent PEG brush in the absence of a lipid membrane. The PEG brush height can be calculated as

$$ h = \left(\frac{\sigma}{3}\right)^{1/3} b^{2/3} aN $$

where σ is the tether density and b = 7.6 Å is the Kuhn length, yielding a brush height of 95 ± 10 Å.[28] The close match between this calculation and the thickness of tether region measured here suggests that the membrane does not constrain or significantly impact the PEG brush structure. However, the grafted polymer brush structure in good solvent may be more accurately described using a parabolic density profile.[29,30] Such a parabolic density distribution is consistent with our observation of a lower degree of hydration within the tether region adjacent to the quartz surface. A parabolic density profile would exhibit a maximum extension 30% greater than the 95 Å brush height calculation used previously. This additional 29 Å extension of low tether density is roughly consistent with the ~25 Å FWHM measured out-of-plane fluctuation of the membrane, modeled as an rms roughness of ~10 Å.

Binding of CTxB to the Tethered Membranes. Biological functionality of the PEG-tethered lipid bilayers was demonstrated by interacting cholera toxin's binding subunit CTxB with ganglioside receptors embedded in the membrane. Ganglioside GM1, a glycosphingolipid with strong specific binding affinity for CTxB,[31] was added to the outer leaflet of a DSPC bilayer at a concentration of 10 mol % to enable high-coverage protein binding. The tethered membrane structure before binding was measured by NR (Figure 4A) in scattering contrasts (i) to (iii): green, red, and blue symbols and lines, respectively. The resulting SLD distributions are shown as dashed lines of corresponding colors in Figure 4B, and the numerical values of the fitting parameters are presented in Table 2. The SLDs indicate the presence of a single bilayer with >90% surface occupancy separated from the
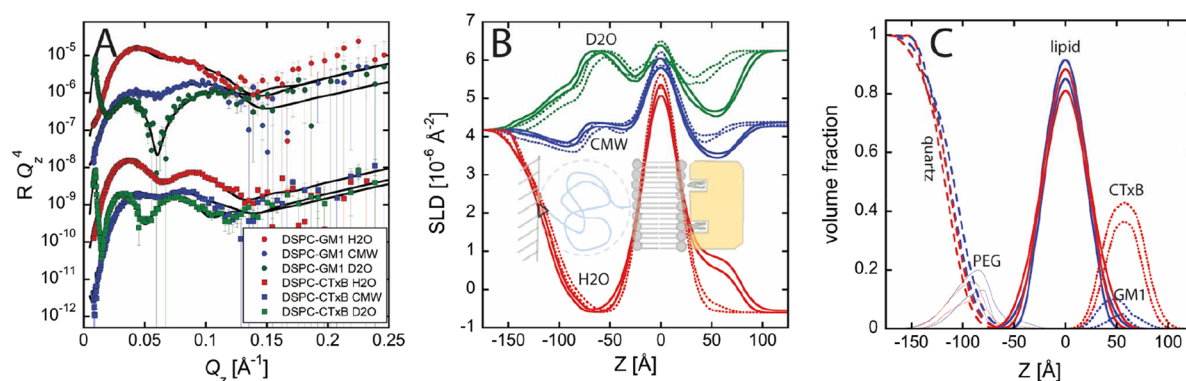
Figure 4. (A) Symbols with error bars show NR data obtained for H_2O (red), D_2O (green), and quartz-matched (blue) contrast conditions for lipopolymer cushioned d-DSPC bilayers containing 10 mol % of ganglioside GM1 in the outer leaflet before (circles) and after (squares) CTxB binding. Solid lines represent best fits to the data corresponding to the SLD and volume fractions presented. Data before CTxB binding is shifted vertically for clarity. (B) SLD profiles obtained from the NR fits before (dashed lines) and after (solid lines) CTxB binding. The same colors are used to indicate the corresponding contrast conditions. Pairs of matched lines define regions of SLD that satisfy the $\chi^2_{min} + 1$ condition and represent the uncertainty of the distribution. A schematic is overlaid with the SLD profile to show the positions of different structural elements of the system. (C) Volume fractions of individual components of the tethered membrane system. Solid lines correspond to the lipid membrane, thin lines correspond to PEG, dashed lines correspond to the substrate and silane layer, and dotted lines correspond to either the GM1 carbohydrates (before binding, blue) or to bound CTxB (after binding, red). The volume fraction of water was not included for clarity.

Table 2. Parameters for Fits to Data Presented in Figure 4[a]

	before CTxB binding: χ^2 = 7.5−8.5			
Z	SLD	solv	σ	
	4.18*	0*	5.0 ± 2	quartz substrate
36.1 ± 3.9	3.94 ± 0.15	11 ± 9	18.0 ± 2.0	silanated surface
36.1 ± 6.7[¥]	0.63*	82 ± 4	9.8 ± 5.0	first PEG region
37.3 ± 6.7[¥]	0.63*	99 ± 1	10.1 ± 1.6	second PEG region
20.1 ± 3.2	2.32 ± 2.2	62 ± 23	10.1[•]	inner lipid HGs
33.0 ± 8.0	6.42 ± 0.35	3 ± 3	10.1[•]	alkyl tail region
20.1[‡]	2.32[‡]	62[‡]	10.1[‡•]	outer lipid HGs
19.8 ± 10.3	0.70 ± 0.80	85 ± 9	10.1[•]	GM1 carbohydrate
	6.25 ± 0.009			D_2O subphase
	4.35 ± 0.04			CMW subphase
	−0.58 ± 0.02			H_2O subphase
	after CTxB binding: χ^2 = 4.1−5.1			
Z	SLD	solv	σ	
	4.18*	0*	5.0 ± 2	quartz substrate
34.6 ± 4.5	4.11 ± 0.06	10 ± 8	17.3 ± 2.3	silanated surface
34.6 ± 3.4[¥]	0.63*	84 ± 3	8.7 ± 3.7	first PEG region
43.5 ± 3.4[¥]	0.63*	100 ± 0	11.2 ± 0.9	second PEG region
22.5 ± 1.8	3.61 ± 0.30	54 ± 7	11.2[•]	inner lipid HGs
27.9 ± 2.9	6.56 ± 0.33	3 ± 3	11.2[•]	alkyl tail region
22.5[‡]	3.61[‡]	54[‡]	11.2[‡•]	outer lipid HGs
42.0 ± 4.0	2.31 ± 0.23	57 ± 3	11.2[•]	CTxB protein
	6.25 ± 0.001			D_2O subphase
	4.31 ± 0.05			CMW subphase
	−0.58 ± 0.02			H_2O subphase

[a]The units of Z, SLD, and roughness σ are in Å, 10^{-6} Å^{-2}, and Å, respectively. Parameter "solv" describes the volume percent of water in the layer.*Values were fixed to theoretical SLDs. [¥]Due to interdependence of the two PEG layer thicknesses, error is given for the total PEG layer. [‡]Fits were constrained to have symmetric lipid headgroups. [•]Roughness of all components of the lipid membrane was constrained to be the same.

quartz support by ∼75 Å, similar to the previously discussed cases with pure DSPC and d-DSPC bilayers. The main difference was a modification of the quartz surface modeled as an additional silanated layer, resulting from the reuse of the

substrate and incomplete removal of the tethering molecules following a previous lipopolymer deposition. As previously discussed, the large lipid head group thickness results from the layer corresponding to a mixture of head groups, water, and lipid tails due to model constraints requiring the layer thickness to be greater than twice the interfacial roughness. Although there is a high uncertainty associated with the GM1 distribution, the SLD distributions clearly identify the GM1 head groups extending 19.8 ± 10.3 Å from the lipid head groups in D_2O and CMW. Assuming an average area per lipid of 46.4 Å^2 and a 1200 Å^3 volume for the polar head group of GM1,[32] the layer corresponds to a 9 ± 7 mol % GM1 content in the outer membrane leaflet and is consistent with the maintenance of 10 mol % GM1 content following LS deposition.

Incubation with CTxB caused significant changes in the NR signals (Figure 4A), most noticeably in the H_2O and D_2O contrast conditions. The resulting SLD profiles obtained from fits to the NR data are shown as solid lines in Figure 4B. CTxB molecules bound to the outer leaflet of the lipid bilayer are readily apparent in the SLD profiles, and the 42 ± 4 Å thickness of this region is consistent with the CTxB crystal structure and orientation of the toxin with the pore axis normal to the membrane plane.[33,34] Volume fractions of the components obtained from the SLD profiles before (blue) and after CTxB binding (red) are shown in Figure 4C. Notably, the binding of CTxB molecules to the PEG tethered bilayer did not cause significant changes to the structure of the hydrated tether region or the bilayer, suggesting that CTxB binding to gel phase membranes does not generate significant membrane curvature.[35] While the GM1 head groups can be identified before protein binding, after toxin binding NR cannot discriminate them from the bound CTxB protein and the parameters describing the layer correspond to the combination of both components. Since this layer is a mixture of GM1 and CTxB, changes in protein SLD due to exchange of labile hydrogens in the different solvents was not explicitly accounted for in the model. To decouple the individual contributions to the parameter values obtained from the

model, the contribution of the GM1 volume fraction and SLD in the mixed layer were determined as

$$\phi'_{GM1} = \phi_{GM1} \cdot \frac{z_{GM1}}{z_{mix}}$$

$$\beta'_{GM1} = \phi'_{GM1} \cdot \beta_{GM1}$$

where ϕ_{GM1}, z_{GM1}, and β_{GM1} are the volume fraction, thickness, and SLD model parameters for the GM1 layer before binding, z_{mix} and β_{mix} are the model parameters for the layer corresponding to a mixture of CTxB and GM1 after binding, and ϕ'_{GM1} and β'_{GM1} are the GM1 contributions to the volume fraction and SLD of the mixed layer, respectively. The volume fraction and SLD of CTxB in the mixed layer is then calculated as

$$\phi_{CTB} = 1 - \phi'_{GM1}$$

$$\beta_{CTB} = \frac{\beta_{mix} - \beta'_{GM1}}{\phi_{CTB}}$$

yielding values of $\phi_{CTB} = 0.4 \pm 0.04$ and $\beta_{CTB} = 2.43 \pm 0.3 \times 10^{-6}$ Å^{-2}. The theoretical SLDs of CTxB at the three different contrasts were estimated by approximating the protein volume using the CTxB crystal structure and a rolling probe method ($r_{probe} = 1.5$ Å; $V_{CTxB} = 75,400$ Å^3) and assuming that H−D exchange with the solvent was limited to 90% of the labile hydrogens.[36,37] This approach resulted in theoretical SLD values of 1.74×10^{-6}, 2.60×10^{-6}, and 2.94×10^{-6} Å^{-2} in H$_2$O, CMW, and D$_2$O, respectively. The average of these SLD values, 2.43×10^{-6} Å^{-2}, is in good agreement with the CTxB SLD obtained from the model.

The CTxB volume fraction (ϕ_{CTB}) was used to approximate the areal coverage of protein bound to the tethered membrane surface (θ_{CTB}) after correcting for the difference in the thickness of the modeled CTxB layer obtained from NR and the projection of the CTxB crystal structure. A Voronoi tessellation method was used to calculate the cross-sectional area of CTxB as a function of distance, Z, along the long axis of the protein's central pore (Figure 5). Voronoi tessellations
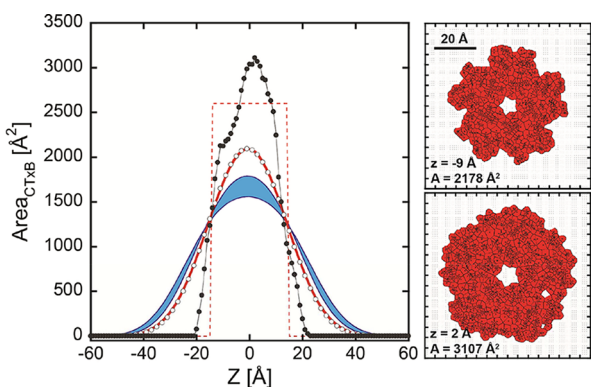
were calculated for a series of 1.5 Å thick slices in Z by projecting all atomic positions from the crystal structure falling within the slice on the X−Y plane and bounding them by a 1 Å grid of points. The cross-sectional area of the slice was calculated as the sum of the areas of all polygons with an atomic position within 1.5 Å of its perimeter. The total CTxB volume calculated by the Voronoi tessellation method was 76,000 Å^3, within 1% of the volume calculated by the rolling ball method. To account for the membrane roughness, the distribution was convolved with a $\sigma = 11.2$ Å Gaussian function (Figure 5, open symbols). An effective layer thickness corresponding to the crystal structure was approximated by convolving a rectangular function with a $\sigma = 11.2$ Å Gaussian function to match the roughness smeared distribution determined by the Voronoi tessellation approach. This resulted in an effective CTxB layer with thickness of 29 Å and an average area of 2600 Å^2 (Figure 5, dashed line). Compared to the effective CTxB layer thickness, the 42 ± 4 Å layer thickness obtained from the NR model suggests either vertical displacement or tilting of the proteins relative to the membrane surface. In either case, accounting for the difference and approximating the membrane surface as a plane, we calculate the surface coverage of bound protein, θ_{CTB}:

$$\theta_{CTB} = \phi_{CTB} \cdot \frac{z_{CTB}}{z_{eff}}$$

where z_{CTB} is the thickness of the CTxB layer obtained from NR and z_{eff} is the effective thickness of the CTxB protein obtained from Voronoi tessellations of the crystal structure. This approach yields a value of 0.58 ± 0.08 coverage of bound protein on the tethered membrane surface. Using twice the receptor concentration, similar coverages of 0.51 ± 0.02 and $0.56 \pm 0.7\%$ were measured for CTxB binding to 20 mol % GM1 in DPPE monolayers at the air−water interface.[2,38]

While far less than either ideal periodic packing[39] (0.907) or random close packing[40] (0.82) of regular circles, the measured protein coverage reported here and in previous work is consistent with simulations of random sequential adsorption of regular circles on a plane (0.547).[41] This suggests that there was insignificant lateral rearrangement of CTxB when bound to receptors in a gel phase membrane to enable higher surface coverage. However, measurements of the lateral diffusion coefficient of GM1 in gel phase membranes[42] and CTxB bound to gel phase membranes[43] are on the order of $D = 1$ μm^2/s, which should provide sufficient mean square displacement of bound proteins within the time scales of the experiment to enable packing rearrangements and higher surface coverage. The saturation of bound protein coverage at values consistent with random sequential adsorption may indicate significant inhibition of the lateral mobility of CTxB, particularly under conditions of membrane crowding.

■ CONCLUSIONS

Using NR, we investigated the structure of lipid bilayers tethered to a quartz surface using triethoxysilane-functionalized PEG lipopolymers. A simple one-step protocol was implemented to functionalize the surface by dissolving the DSPE−PEG$_{75}$−silane lipopolymers in 1:1 EtOH:MeOH and incubating the solution in contact with monocrystalline quartz. Subsequent lipid deposition by Langmuir−Blodgett/Langmuir−Schaefer (LB/LS) deposition was used to complete the tethered bilayer. When sufficiently long incubation times (here >12 h) were used, the lipid bilayer was uniformly

Figure 5. Cross-sectional area of CTxB as a function of Z. Solid symbols represent the areas obtained from Voronoi tessellations of slices through the CTxB crystal structure, and open symbols represent the areas after accounting for the membrane roughness ($\sigma = 11.2$ Å). The dashed red line is a box function ($z = 29$ Å) that best reproduces the CTxB areas after accounting for membrane roughness (solid red line). The shaded blue region corresponds to the CTxB distribution from the NR model. Panels to the right show representative Voronoi tessellations of slices through the CTxB structure.

separated from the surface by highly hydrated PEG tethers. NR results showed that the PEG tethers were 90% hydrated and formed a ~95 Å thick cushion, which supported a high coverage bilayer with 10−15 Å rms. roughness. Surprisingly, capping the grafted PEG brush with a gel-phase lipid bilayer has minimal impact on the brush's conformation. Using interactions between CTxB and its glycosphingolipid receptor GM1, we demonstrate that the tethered lipid bilayer system described here is well suited to be a platform for studies of protein−lipid interactions. Efficient CTxB binding to GM1 in the outer leaflet resulted in coverage of the CTxB protein layer of θ_{CTB} = 0.58 ± 0.08, consistent with random sequential adsorption of proteins to the membrane surface. Under the conditions studied, binding resulted in minimal perturbation to the tethered lipid membrane conformation, providing insight into the limits of a CTxB-mediated mechanism in generating membrane curvature.

■ AUTHOR INFORMATION

Corresponding Author

Erik B. Watkins − *MPA-11: Materials Synthesis and Integrated Devices, Los Alamos National Laboratory, Los Alamos, New Mexico 87545, United States; Institut Laue-Langevin, 38042 Grenoble, France;* ● orcid.org/0000-0001-8573-9629; Email: ebw@lanl.gov

Authors

Andrew J. C. Dennison − *Dept. Physics and Astronomy, University of Sheffield, Sheffield S3 7HG, U.K.*

Jaroslaw Majewski − *Division of Molecular and Cellular Biosciences, National Science Foundation, Alexandria 22303 Virginia, United States; Theoretical Biology and Biophysics at Los Alamos National Laboratory, Los Alamos National Laboratory, Los Alamos, New Mexico 87545, United States; Department of Chemical and Biological Engineering and Center for Biomedical Engineering, University of New Mexico, Albuquerque, New Mexico 87131, United States*

Complete contact information is available at:
https://pubs.acs.org/10.1021/acs.langmuir.2c00499

Notes

The authors declare no competing financial interest.

■ ACKNOWLEDGMENTS

■ REFERENCES

(1) Watkins, E. B.; Miller, C. E.; Majewski, J.; Kuhl, T. L. Membrane texture induced by specific protein binding and receptor clustering: active roles for lipids in cellular function. *Proc. Natl. Acad. Sci. U. S. A.* **2011**, *108*, 6975−6980.

(2) Miller, C. E.; Majewski, J.; Watkins, E. B.; Kuhl, T. L. Part I: An x-ray scattering study of cholera toxin penetration and induced phase transformations in lipid membranes. *Biophys. J.* **2008**, *95*, 629−640.

(3) Miller, C. E.; Majewski, J.; Watkins, E. B.; Weygand, M.; Kuhl, T. L. Part II: Diffraction from two-dimensional cholera toxin crystals bound to their receptors in a lipid monolayer. *Biophys. J.* **2008**, *95*, 641−647.

(4) Borch, J.; Hamann, T. The nanodisc: a novel tool for membrane protein studies. *Biol. Chem.* **2009**, *390*, 805−814.

(5) Denisov, I. G.; Sligar, S. G. Nanodiscs in Membrane Biochemistry and Biophysics. *Chem. Rev.* **2017**, *117*, 4669−4713.

(6) Chenal, A.; Prongidi-Fix, L.; Perier, A.; Aisenbrey, C.; Vernier, G.; Lambotte, S.; Haertlein, M.; Dauvergne, M. T.; Fragneto, G.; Bechinger, B.; Gillet, D.; Forge, V.; Ferrand, M. Corrigendum to "Deciphering Membrane Insertion of the Diphtheria Toxin T Domain by Specular Neutron Reflectometry and Solid-State NMR Spectroscopy" [J. Mol. Biol. (2009) 391, 872−883]. *J. Mol. Biol.* **2009**, *394*, 587−587.

(7) Vacklin, H. P.; Tiberg, F.; Fragneto, G.; Thomas, R. K. Phospholipase A₂ hydrolysis of supported phospholipid bilayers: A neutron reflectivity and ellipsometry study. *Biochemistry* **2005**, *44*, 2811−2821.

(8) Soranzo, T.; Martin, D. K.; Lenormand, J. L.; Watkins, E. B. Coupling neutron reflectivity with cell-free protein synthesis to probe membrane protein structure in supported bilayers. *Sci. Rep.* **2017**, *7*, 3399.

(9) Penkauskas, T.; Preta, G. Biological applications of tethered bilayer lipid membranes. *Biochimie* **2019**, *157*, 131−141.

(10) Kendall, J. K. R.; Johnson, B. R. G.; Symonds, P. H.; Imperato, G.; Bushby, R. J.; Gwyer, J. D.; van Berkel, C.; Evans, S. D.; Jeuken, L. J. C. Effect of the Structure of Cholesterol-Based Tethered Bilayer Lipid Membranes on Ionophore Activity. *ChemPhysChem* **2010**, *11*, 2191−2198.

(11) Castellana, E. T.; Cremer, P. S. Solid supported lipid bilayers: From biophysical studies to sensor design. *Surf. Sci. Rep.* **2006**, *61*, 429−444.

(12) Sackmann, E.; Tanaka, M. Supported membranes on soft polymer cushions: fabrication, characterization and applications. *Trends Biotechnol.* **2000**, *18*, 58−64.

(13) Tanaka, M.; Sackmann, E. Polymer-supported membranes as models of the cell surface. *Nature* **2005**, *437*, 656−663.

(14) Wagner, M. L.; Tamm, L. K. Tethered polymer-supported planar lipid bilayers for reconstitution of integral membrane proteins: Silane-polyethyleneglycol-lipid as a cushion and covalent linker. *Biophys. J.* **2000**, *79*, 1400−1414.

(15) Kiessling, V.; Tamm, L. K. Measuring distances in supported bilayers by fluorescence interference-contrast microscopy: Polymer supports and SNARE proteins. *Biophys. J.* **2003**, *84*, 408−418.

(16) Majewski, J.; Wong, J. Y.; Park, C. K.; Seitz, M.; Israelachvili, J. N.; Smith, G. S. Structural studies of polymer-cushioned lipid bilayers. *Biophys. J.* **1998**, *75*, 2363−2367.

(17) Naumann, C. A.; Prucker, O.; Lehmann, T.; Rühe, J.; Knoll, W.; Frank, C. W. The polymer-supported phospholipid bilayer: Tethering as a new approach to substrate-membrane stabilization. *Biomacromolecules* **2002**, *3*, 27−35.

(18) Watkins, E. B.; El-Khouri, R. J.; Miller, C. E.; Seaby, B. G.; Majewski, J.; Marques, C. M.; Kuhl, T. L. Structure and Thermodynamics of Lipid Bilayers on Polyethylene Glycol Cushions: Fact and Fiction of PEG Cushioned Membranes. *Langmuir* **2011**, *27*, 13618−13628.

(19) Maccarini, M.; Gayet, L.; Alcaraz, J. P.; Liguori, L.; Stidder, B.; Watkins, E. B.; Lenormand, J. L.; Martin, D. K. Functional Characterization of Cell-Free Expressed OprF Porin from Pseudomonas aeruginosa Stably Incorporated in Tethered Lipid Bilayers. *Langmuir* **2017**, *33*, 9988−9996.

(20) Köhler, S.; Fragneto, G.; Alcaraz, J.-P.; Nelson, A.; Martin, D. K.; Maccarini, M. Nanostructural Characterization of Cardiolipin-Containing Tethered Lipid Bilayers Adsorbed on Gold and Silicon Substrates for Protein Incorporation. *Langmuir* **2021**, *37*, 8908−8923.

(21) Andersson, J.; Fuller, M. A.; Wood, K.; Holt, S. A.; Köper, I. A tethered bilayer lipid membrane that mimics microbial membranes. *Phys. Chem. Chem. Phys.* **2018**, *20*, 12958−12969.

(22) Bilotto, P.; Lengauer, M.; Andersson, J.; Ramach, U.; Mears, L. L. E.; Valtiner, M. Interaction Profiles and Stability of Rigid and Polymer-Tethered Lipid Bilayer Models at Highly Charged and Highly Adhesive Contacts. *Langmuir* **2019**, *35*, 15552−15563.

(23) Andersson, J.; Köper, I.; Knoll, W. Tethered Membrane Architectures-Design and Applications. *Front. Mater.* **2018**, *5*, 11.

(24) Tamm, L. K.; McConnell, H. M. SUPPORTED PHOSPHO-LIPID-BILAYERS. *Biophys. J.* **1985**, *47*, 105−113.

(25) Campbell, R. A.; Wacklin, H. P.; Sutton, I.; Cubitt, R.; Fragneto, G. FIGARO: The new horizontal neutron reflectometer at the ILL. *Eur. Phys. J. Plus* **2011**, *126*, 107.

(26) Parratt, L. G. Surface Studies of Solids by Total Reflection of X-Rays. *Phys. Rev.* **1954**, *95*, 359−369.

(27) Watkins, E. B.; Gao, H.; Dennison, A. J. C.; Chopin, N.; Struth, B.; Arnold, T.; Florent, J.-C.; Johannes, L. Carbohydrate Conformation and Lipid Condensation in Mono layers Containing Glycosphingolipid Gb3: Influence of Acyl Chain Structure. *Biophys. J.* **2014**, *107*, 1146−1155.

(28) Emilsson, G.; Schoch, R. L.; Feuz, L.; Höök, F.; Lim, R. Y. H.; Dahlin, A. B. Strongly Stretched Protein Resistant Poly(ethylene glycol) Brushes Prepared by Grafting-To. *ACS Appl. Mater. Interfaces* **2015**, *7*, 7505−7515.

(29) Milner, S. T.; Witten, T. A.; Cates, M. E. A PARABOLIC DENSITY PROFILE FOR GRAFTED POLYMERS. *Europhys. Lett.* **1988**, *5*, 413−418.

(30) Milner, S. T. POLYMER BRUSHES. *Science* **1991**, *251*, 905−914.

(31) Kuziemko, G. M.; Stroh, M.; Stevens, R. C. Cholera toxin binding affinity and specificity for gangliosides determined by surface plasmon resonance. *Biochemistry* **1996**, *35*, 6375−6384.

(32) Marsh, D. Molecular volumes of phospholipids and glycolipids in membranes. *Chem. Phys. Lipids* **2010**, *163*, 667−677.

(33) Zhang, R. G.; Westbrook, M. L.; Westbrook, E. M.; Scott, D. L.; Otwinowski, Z.; Maulik, P. R.; Reed, R. A.; Shipley, G. G. The 2.4 Å Crystal Structure of Cholera Toxin B Subunit Pentamer: Choleragenoid. *J. Mol. Biol.* **1995**, *251*, 550−562.

(34) Merritt, E. A.; Kuhn, P.; Sarfaty, S.; Erbe, J. L.; Holmes, R. K.; Ho, W. G. J. The 1.25 Å resolution refinement of the cholera toxin B-pentamer: evidence of peptide backbone strain at the receptor-binding site. *J. Mol. Biol.* **1998**, *282*, 1043−1059.

(35) Kabbani, A. M.; Raghunathan, K.; Lencer, W. I.; Kenworthy, A. K.; Kelly, C. V. Structured clustering of the glycosphingolipid GM1 is required for membrane curvature induced by cholera toxin. *Proc. Natl. Acad. Sci. U. S. A.* **2020**, *117*, 14978−14986.

(36) Bouwman, W. G. On the scattering length density of proteins in H_2O/D_2O: Determination of H-D exchange using ES^+I-MS. *J. Radioanal. Nucl. Chem.* **2005**, *264*, 271−275.

(37) Voss, N. R.; Gerstein, M. 3V: cavity, channel and cleft volume calculator and extractor. *Nucleic Acids Res.* **2010**, *38*, W555−W562.

(38) Miller, C. E.; Majewski, J.; Kjaer, K.; Weygand, M.; Faller, R.; Satija, S.; Kuhl, T. L. Neutron and X-ray scattering studies of cholera toxin interactions with lipid monolayers at the air-liquid interface. *Colloids Surf., B* **2005**, *40*, 159−163.

(39) Fejes, L. Über die dichteste Kugellagerung. *Math. Z.* **1942**, *48*, 676−684.

(40) Berryman, J. G. Random close packing of hard spheres and disks. *Phys. Rev. A* **1983**, *27*, 1053−1061.

(41) Feder, J. Random Sequential Adsorption. *J. Theor. Biol.* **1980**, *87*, 237−254.

(42) Goins, B.; Masserini, M.; Barisas, B. G.; Freire, E. Lateral Diffusion of Ganglioside-Gm1 in Phospholipid-Bilayer Membranes. *Biophys. J.* **1986**, *49*, 849−856.

(43) Forstner, M. B.; Yee, C. K.; Parikh, A. N.; Groves, J. T. Lipid lateral mobility and membrane phase structure modulation by protein binding. *J. Am. Chem. Soc.* **2006**, *128*, 15221−15227.